

**SYNTHESIS AND CHARACTERIZATION OF
MULTI-DOPED (Mg^{2+} , Si^{4+} , Cu^{2+} , Fe^{3+})
CARBONATED HYDROXYAPATITE VIA
NANOEMULSION METHOD**

ILIYA EZEKIEL

UNIVERSITI SAINS MALAYSIA

2018

**SYNTHESIS AND CHARACTERIZATION OF MULTI-DOPED (Mg^{2+} , Si^{4+} ,
 Cu^{2+} , Fe^{3+}) CARBONATED HYDROXYAPATITE VIA NANOEMULSION
METHOD**

by

ILIYA EZEKIEL

**Thesis submitted in partial fulfillment of the
requirements for the degree of
Master of Science**

November 2018

DECLARATION

I hereby declare that I have conducted, completed the research work and written the dissertation entitled “Synthesis and Characterization of Multidoped (Mg^{2+} , Si^{4+} , Cu^{2+} , Fe^{3+}) Carbonated Hydroxyapatite via Nanoemulsion Route”. I also declare that it has not been previously submitted for the award for any degree or diploma or other similar title for any other examining body or university.

Name of student : ILIYA EZEKIEL

Signature:

Date: : 8th August 2018

Witness by

Supervisor : Prof. Dr. AHMAD-FAUZI MOHD NOOR

Signature:

Date: : 8th August 2018

ACKNOWLEDGEMENT

The author wishes to acknowledge with immense gratitude, his supervisor, Prof. Dr. Ahmad Fauzi Mohd Noor, for his support, assistance and encouragement throughout the course of the research work. The author is indebted and grateful to his co-supervisors, Dr. Shah Rizal Kasim and Dr. Yanny Marliana Baba Ismail for their assistance, continuous support and personal involvements in all the aspects of this Master research. Working with them was an opportunity for great learning and experience. The author would also like to extend his gratitude to all the technical staff of the School of Materials and Mineral Resources Engineering, Univeristi Sains Malaysia, most especially, Encik Mokhtar Bin Mohamad, Encik Kemuridan Bin Md. Desa, Encik Muhammad Khairi Bin Khalid, Encik Abdul Rashid Bin Selamat and Encik Mohammad Azrul Bin Zainol Abidin for making available the needed facilities in the accomplishment of this research work.

The author would also like to thank specially his parents and sibling for their prayers, his lovely wife, Esther and wonderful children, Seth, Jason and Vida for their constant prayers, guidance, encouragement, and support. To all my friends all over the world and in Nigerian, I say thank you all for being there for me. Finally, the author would like to thank his research group members for being the best buddies.

Best wishes

ILIYA EZEKIEL

November 2018

TABLE OF CONTENTS

	Page
ACKNOWLEDGEMENT	ii
TABLE OF CONTENTS	iii
LIST OF TABLES	vii
LIST OF FIGURES	ix
LIST OF ABBREVIATIONS	xiii
LIST OF SYMBOLS	xv
ABSTRAK	xvii
ABSTRACT	xix
CHAPTER ONE: INTRODUCTION	
1.1 Research background	1
1.2 Problem statement	5
1.3 Scope of study	6
1.4 Research objectives	8
1.5 Thesis outline	8
CHAPTER TWO: LITERATURE REVIEW	
2.1 Introduction	9
2.1.1 Bone	10
2.1.2 Composition of bone	11
2.1.3 Macrostructure of bone	12
2.1.4 Microstructure of bone	13
2.1.5 Nanostructure of bone	14
2.1.6 Bone cell	15
2.1.6 (a) Osteoblasts, osteoclasts and osteocytes	15
2.1.7 Biomechanical properties of bone	16
2.2 Types of bone substitute	18
2.2.1 Bone Graft Substitute (BGs)	19
2.2.2 Autograft bone graft	21
2.2.3 Allograft bone graft	21
2.2.4 Xenograft bone graft	22

2.2.5	Synthetic bone graft	22
2.3	Biomaterials	23
2.3.1	Properties of biomaterials	25
2.3.1(a)	Physical properties	25
2.3.1 (b)	Mechanical properties	26
2.3.1 (c)	Chemical properties	26
2.3.1 (d)	Biological properties	27
2.4	Bioceramics	28
2.4.1	Classification of bioceramics	28
2.4.2	Calcium phosphate (CaP) bioceramics	29
2.4.3	Hydroxyapatite, HA	31
2.4.4	Synthesis of hydroxyapatite, HA	33
2.4.5	Substituted hydroxyapatite, HA	34
2.4.5 (a)	Anionic substitution of hydroxyapatite, HA	37
2.4.5 (a) (i)	Carbonate (CO_3^{2-})	37
2.4.5 (a) (ii)	Silicate (SiO_4^{4-})	40
2.4.5 (b)	Other anionic substitution	41
2.4.5 (c)	Cationic substitution of hydroxyapatite, HA	42
2.4.5 (c) (i)	Magnesium (Mg^{2+})	42
2.4.5 (c) (ii)	Iron (Fe^{3+})	43
2.4.5 (c) (iii)	Copper (Cu^{2+})	43
2.4.5 (d)	Other cationic substitution of hydroxyapatite, HA	44
2.4.5 (e)	Multi-ionic substitution of hydroxyapatite, HA	45
2.5	Sintering	46
2.5.1	Sintering variables	48
2.5.2	Sintering process variable	49
2.5.3	Sintering material variables	50
2.5.4	Sintering additives	51
2.5.5	Sintering of carbonated hydroxyapatite	52
CHAPTER THREE: MATERIALS AND METHODS		
3.1	Introduction	53
3.2	Synthesis of multi-doped carbonated hydroxyapatite	54
3.3	Preparation of sintered multi-doped carbonated HA pellets	59

3.3.1	Dry pressing	59
3.4	Sintering of multi-doped carbonated CHAII pellets	60
3.5	Carbonate (CO_3^{2-}) recompensating from wet carbon dioxide (CO_2)	61
3.6	Characterization	64
3.6.1	X-Ray Diffraction (XRD)	64
3.6.2	Fourier Transform Infra-Red (FTIR) Spectroscopy	64
3.6.3	Field Emission Scanning Electron Microscopy (FESEM)	65
3.6.4	Energy Disperse X-Ray Spectroscopy (EDS)	66
3.6.5	Transmission Electron Microscopy (TEM)	67
3.6.6	Carbon Hydrogen Nitrogen/Sulphur (CHN/S)	67
3.6.7	X-Ray Fluorescence (XRF)	68
3.6.8	Specific Surface Area (SSA)	69
3.6.9	Linear shrinkage	70
3.6.10	Density, water absorption and porosity of the sintered pellets	70
3.6.11	Diametral Tensile Strength (DTS)	73
3.6.12	Hardness	75
3.7	Evaluation of <i>in vitro</i> bioactivity	77
3.7.1	Preparation of Simulated Body Fluid (SBF)	77
3.7.2	Immersion of powder and sintered pellets in SBF	78
CHAPTER FOUR: RESULTS AND DISCUSSION		
4.1	Introduction	81
4.2.1	XRD of synthesized powders	82
4.2.2	FTIR analysis	87
4.2.3	Elemental analysis	90
4.2.4	FESEM and EDS Analysis	91
4.2.5	TEM analysis	92
4.2.6	BET surface area analysis	96
4.3	<i>In vitro</i> bioactivity of as-synthesized nanopowders in simulated body fluid (SBF)	97
4.3.1	Apatite formation on as-synthesized nanopowders	97
4.3.2	Ion release of as-synthesized nanopowders	100
4.4	Characterization of sintered pellets	106
4.4.1	XRD analysis of sintered pellets	106

4.4.2	FTIR sintered pellets	111
4.4.3	XRF of sintered pellets	112
4.5	Mechanical properties	117
4.5.1	Linear shrinkage	117
4.5.2	Density, water absorption, porosity and strength (DTS)	119
4.6	Bioactivity of sintered samples	124
4.6.1	Apatite formation	124
4.6.2	Ion release of sintered pellets	128

CHAPTER FIVE: CONCLUSION AND RECOMMENDATION

5.1	Conclusion	133
5.2	Recommendation for future research	135

REFERENCES	137
-------------------	-----

APPENDICES

Appendix A: Stoichiometric calculation of the chemical reaction

Appendix B: Carbonate content obtained from CHN/S of the as-synthesized powders

Appendix C: Yield obtained from synthesis of the as-synthesized CHAI powder

LIST OF PUBLICATIONS

LIST OF TABLES

	Page
Table 2.1 Human cortical and trabecular bone: selected mechanical properties	17
Table 2.2 Summary of biological properties of natural bone grafts and bone substitutes in the clinical application	20
Table 2.3 Various orthophosphates CaP bioceramics ordered by the Ca/P molar ratio	30
Table 2.4 Summary of various synthesis methods and characteristics	34
Table 2.5 Composition and lattice parameters of human bone compared with stoichiometric HA	35
Table 2.6 Substitutions and the effect on lattice axes and solubility of the produced apatite	37
Table 2.7 Difference between A and B- type carbonated HA	38
Table 2.8 Some recent multi-substituted HA reports and findings	45
Table 3.1 Summary of acronyms and phase formula use in synthesis	55
Table 3.2 Chemical reagents and solvents employed in nanoemulsion synthesis and their roles	56
Table 3.3 Summary of concentrations of chemical precursor materials	59
Table 3.4 Chemical reagents for the preparation of 1L SBF solution	77
Table 4.1 Synthesis yield of powder samples: theoretical yields (Y_{th}), actual yields (Y_{at}) and percentage of yield (Y_{pt})	81
Table 4.2 Structure properties of the referenced HA, control and multi-doped carbonated HA powders	83
Table 4.3 FTIR functional groups and assigned wave bands of the as-synthesized nanopowders	90
Table 4.4 XRF analysis of compositions and Ca/P ratios of all the as-synthesized powders	88
Table 4.5 TEM of the as-synthesized powders with variant [nCO_3^{2-}/nPO_4^{3-}] molar ratios	96
Table 4.6 BET specific surface area and derived particle size of the as-synthesized nanopowders	97

Table 4.7	Crystal features of samples sintered at variant temperatures and recompensed with wet CO ₂ at 250 °C	110
Table 4.8	Chemical composition of sintered multi-doped CHAlI pellets	113
Table 4.9	Percentage of linear of shrinkage in diameter (S_d) and thickness (S_t) experimental data and variants sintering temperatures	118
Table 4.10	Density and water absorption of sintered pellets at different temperatures	120
Table 4.11	Porosity relationship of sintered samples at variant temperature	120
Table 4.12	Diametral tensile strength and hardness of sintered compositions	122

LIST OF FIGURES

		Page
Figure 1.1	Flow chart of the research containing three stages of execution	7
Figure 2.1	Generation of biomaterials and timelines	9
Figure 2.2	Displayed matrix of organic and inorganic component of bone composition	11
Figure 2.4	The macro to sub-nanostructure ordered arrangement of the human bone	13
Figure 2.5	Classification of bone cells: osteocyte, osteoblast and osteoclast	16
Figure 2.6	Requisite criteria for ideal biomaterials: bioactive, biodegradable, strength, fabricability and cytocompatibility	24
Figure 2.7	Structure of HA showing its <i>c</i> -axis perpendicular to three <i>a</i> -axes lying at 120° angles to each other(left), with projection on the (001) plane of HA structure (right)	32
Figure 2.8	Type-A, B and AB carbonated hydroxyapatite substitution	37
Figure 2.9	Bi-spherical sintering model: stages of conjoined spheres particle evolution	47
Figure 2.10	Diffusion paths for densification and coarsening for an idealized situation of two spherical particles in contact	48
Figure 2.11	Sintered density time curves illustrating effects of increasing green density and sintering temperature on densification	49
Figure 3.1	Flowchart of the procedure for the synthesis of carbonated HA nanopowders by nanoemulsion route	57
Figure 3.2	Filtration set-up for nanoemulsion synthesis	58
Figure 3.3	Schematics of mould and hydraulic hand press set-up	60
Figure 3.4	Sintering schedule employed in the sintering of multi-doped carbonated HA pellets	61
Figure 3.5	Schematic of carbonate recompensating of sintered carbonated HA pellets by wet CO ₂	62
Figure 3.6	Systematic approach in sintering and wet CO ₂ recompensating of multi-doped carbonated HA pellets at variant temperatures	63

Figure 3.7	Density apparatus set-up based on ASTM C830-00 (Archimedes principle)	71
Figure 3.8	Geometry and parameters of a typical diametral tensile strength test on (a) a cylindrical specimen of a brittle material, and (b) its corresponding FE model with three planes of symmetry. Direction of tensile stress: $x = z = 0$, $y =$ maximum stress, D ; diameter and t ; thickness	74
Figure 3.9	Vickers hardness profile showing Vickers indentation and measurement of impression diagonals	75
Figure 3.10	Graphical representation of sintered multi-doped carbonated HA immersed into SBF solution	79
Figure 4.1	Phase properties of nanopowders: (left) XRD patterns of (a) commercial HA (b) CHAI (c) Mg-Si-CHAI (d) Mg-Si-Cu-CHAI (e)Mg-Si-Fe-CHAI; (right) enlarged XRD patterns at 2θ : 25–35° showing peak shift at (200) and (300) and crystalline phase by intensity of hollow (I_h) between (112) and (300) reflections	83
Figure 4.2	Phase properties of nanopowders: (left) XRD patterns of (a)commercial HA (b) CHAII (c) Mg-Si-CHAII (d)Mg-Si-Cu-CHAII (e) Mg-Si-Fe-CHAII; (right) enlarged XRD patterns at 2θ : 25–35° showing amorphous phase with absence of intensity of hollow (I_h)between (112) and (300) reflections	84
Figure 4.3	Peak height (counts) of commercial HA, CHA and multi-doped CHA nanopowders for both parameters	87
Figure 4.4	FTIR bands of commercial HA, the as-synthesized control CHAI, and multi-doped CHAI	88
Figure 4.5	FTIR bands of commercial HA, the as-synthesized control CHAII, commercial HA and multi-doped CHAII samples	89
Figure 4.6	FESEM micrographs and EDS chemical composition for the as-synthesized nanopowders: (a) CHAI (b) Mg-Si-CHAI (c) Mg-Cu-Si-CHAI (d) Mg-Si-Fe-CHAI	93
Figure 4.7	FESEM micrographs and EDS chemical composition for the as-synthesized nanopowders: (a) CHAII (b) Mg-Si-CHAII (c) Mg-Cu-Si-CHAII (d) Mg-Si-Fe-CHAII	94
Figure 4.8	TEM micrographs of the as synthesized nanopowders: (a) CHAI (b) Mg-Si-CHAI (c) Mg-Cu-Si-CHAI (d) Mg-Si-Fe-CHAI (e) CHAII (f) Mg-Si-CHAII (g) Mg-Cu-Si-CHAII (h) Mg-Si-Fe-CHAII	95

Figure 4.9	FESEM micrographs of in vitro bioactivity study of as-synthesized powders after 7, 14 and 21 days respectively: (a) CHAI (b) Mg-Si-CHAI (c) Mg-Cu-Si-CHAI (d) Mg-Si-Fe-CHAI	98
Figure 4.10	FESEM micrographs of in vitro bioactivity study of as-synthesized powders after 7, 14 and 21 days: (a) CHAII (b) Mg-Si-CHAII (c) Mg-Si-Cu-CHAII (d) Mg-Si-Fe-CHAII	99
Figure 4.11	The amount Ca ions release after 21 days in SBF solution from as-synthesized nanopowders with variant $[n\text{CO}_3^{2-}/n\text{PO}_4^{3-}]$ molar ratio; 0.67 and 1.00: (a) CHA (b) Mg-Si-CHA (c) Mg-Si-Cu-CHA (d) Mg-Si-Fe-CHA	101
Figure 4.12	The amount P ions release after 21 days in SBF solution from as-synthesized nanopowders with variant $[n\text{CO}_3^{2-}/n\text{PO}_4^{3-}]$ molar ratio; 0.67 and 1.00: (a) CHA (b) Mg-Si-CHA (c) Mg-Si-Cu-CHA (d) Mg-Si-Fe-CHA	102
Figure 4.13	The amount Mg ions release after 21 days in SBF solution from as-synthesized nanopowders with variant $[n\text{CO}_3^{2-}/n\text{PO}_4^{3-}]$ molar ratio; 0.67 and 1.00: (a) Mg-Si-CHA (b) Mg-Si-Cu-CHA (c) Mg-Si-Fe-CHA	103
Figure 4.14	The amount Cu^{2+} and Fe^{3+} ions release after 21 days in SBF solution from as synthesized nanopowders with variant $[n\text{CO}_3^{2-}/n\text{PO}_4^{3-}]$ molar ratio; 0.67 and 1.00: (a) Mg-Si-Cu-CHAI and Mg-Si-Cu-CHAII (b) Mg-Si-Fe-CHAI and Mg-Si-Fe-CHAII	104
Figure 4.15	pH values of as-synthesized powders of $[n\text{CO}_3^{2-}/n\text{PO}_4^{3-}] = 0.67$ (left) and 1.00 (right) after soaking in SBF media: (a) CHA (b) Mg-Si-CHA (c) Mg-Si-Cu-CHA (d) Mg-Si-Fe-CHA	105
Figure 4.16	XRD profile of samples sintered at 750 °C and recompensed with wet CO_2 during cooling around 250 °C: (a) CHAII (b) Mg-Si-CHAII (c) Mg-Si-Cu-CHAII (d) Mg-Si-Fe-CHAII	107
Figure 4.17	XRD profile of samples sintered at 800 °C and recompensed with wet CO_2 during cooling around 250 °C: (a) CHAII (b) Mg-Si-CHAII (c) Mg-Si-Cu-CHAII (d) Mg-Si-Fe-CHAII	107
Figure 4.18	XRD profile of samples sintered at 850 °C and recompensed with wet CO_2 during cooling around 250 °C: (a) CHAII (b) Mg-Si-CHAII (c) Mg-Si-Cu-CHAII (d) Mg-Si-Fe-CHAII	108
Figure 4.19	Effect of sintering temperatures on crystallite size for various samples evacuated at 250 °C and recompensed with wet CO_2 in a desiccator for 20 minutes	111
Figure 4.20	FTIR of sintered samples at 800 °C: (a) CHAII (b) Mg-Si-CHAII (c) Mg-Si-Cu-CHAII (d) Mg-Si-Fe-CHAII	112

Figure 4.21	FESEM micrographs of 35 % H ₃ PO ₄ (60 sec.) etched surface section of pellets sintered at 750 °C: (a) CHAII (b) Mg-Si-CHAII (b) Mg-Si-Cu-CHAII (d) Mg-Si-Fe-CHAII	115
Figure 4.22	FESEM micrographs of 35 % H ₃ PO ₄ (60 sec.) etched surface section of pellets sintered at 800°C: (a) CHAII (b) Mg-Si-CHAII (b) Mg-Si-Cu-CHAII (d) Mg-Si-Fe-CHAII	116
Figure 4.23	FESEM micrographs of 35 % H ₃ PO ₄ (60 sec.) etched surface section of pellets sintered at 850°C: (a) CHAII (b) Mg-Si-CHAII (b) Mg-Si-Cu-CHAII (d) Mg-Si-Fe-CHAII	116
Figure 4.24	Linear shrinkage of pelletized samples at sintering temperatures 750°C, 800°C and 850°C: (a) % of linear of shrinkage in diameter, S_d (b) % of linear of shrinkage in thickness, S_t	117
Figure 4.25	Relative density (D_r) and open porosity (P_o) at different sintering temperatures	121
Figure 4.26	Strength and hardness performance of sintered samples at different temperatures: (a) DTS vs temperature (b) H_v vs temperature	123
Figure 4.27	Micrographs of samples at 800 °C with apatite forming ability after day 7: at 5KX mag. (a) CHAII (b) Mg-Si-CHAII (c) Mg-Si-Cu-CHAII (d) Mg-Si-Fe-CHAII and at 10 KX mag. (e) CHAII (f) Mg-Si-CHAII (g) Mg-Si-Cu-CHAII (h) Mg-Si-Fe-CHAII	125
Figure 4.28	Micrographs of samples at 800 °C with apatite forming ability after day 14: at 5KX mag. (a) CHAII (b) Mg-Si-CHAII (c) Mg-Si-Cu-CHAII (d) Mg-Si-Fe-CHAII and at 10 KX mag. (e) CHAII (f) Mg-Si-CHAII (g) Mg-Si-Cu-CHAII (h) Mg-Si-Fe-CHAII	126
Figure 4.29	Micrographs of samples at 800 °C with apatite forming ability after day 21: at 5KX mag. (a) CHAII (b) Mg-Si-CHAII (c) Mg-Si-Cu-CHAII (d) Mg-Si-Fe-CHAII and at 10 KX mag. (e) CHAII (f) Mg-Si-CHAII (g) Mg-Si-Cu-CHAII (h) Mg-Si-Fe-CHAII	127
Figure 4.30	Ion release kinetics of Ca ²⁺ in control CHAII and multi-doped CHAII sintered at 800 °C	128
Figure 4.31	Ion release kinetics of P ²⁺ in control CHAII and multi-doped CHAII sintered at 800 °C	129
Figure 4.32	Ion release kinetics of Mg ²⁺ in multi-doped CHAII at 800 °C	130
Figure 4.33	Ion release kinetics of Cu ²⁺ and Fe ³⁺ in multi-doped CHAII sintered at 800 °C	131
Figure 4.34	pH profile of the control CHAII and multi-doped CHAII sintered at 800 °C	132

LIST OF ABBREVIATIONS

BET	Bruanauer, Emmett and Teller
BGS	Bone Graft Substitute
Ca ²⁺	Calcium ion
CaO	Calcium oxide
Ca/P	Calcium/Phosphate ratio
CaP	Calcium phosphate
CDHA	Calcium-deficient Hydroxyapatite
CHAI	Carbonated hydroxyapatite I
CHAI	Carbonated hydroxyapatite II
CHN/S	Carbon, hydrogen, nitrogen and sulphur
CO ₂	Carbon Dioxide
Cu ²⁺	Copper ion
DI	De-ionised
DTS	Diametral Tensile Strength
FTIR	Fourier Transform Infrared Spectroscopy
FWHM	Full width at half maximum
HA	Hydroxyapatite
ICDD	International Centre for Diffraction Data

Fe ³⁺	Iron ion
ICP-OES	Inductively coupled plasma optical electron spectrometry
Mg ⁺²	Magnesium ion
Mg-Si-CHA	Magnesium, silicon and carbonate doped HA
Mg-Si-Cu-CHA	Magnesium, silicon, copper and carbonate doped HA
Mg-Si-Fe-CHA	Magnesium, silicon, Fe and carbonate doped HA
Si ⁴⁺	Silicon ion
SBF	Simulated body fluid
TEM	Transmission Electron Microscope
XRD	X-ray Diffraction
XRF	X-ray Fluorescence

LIST OF SYMBOLS

Å	Angstrom
cm	centimeter
°C	Degree Celsius
°/min	Degree/minute
ρ	Density
g	Gram
h	Hour
I_h	Intensity of hollow
<	Less than
m	Meter
MPa	Mega Pascal = 1 N/mm ²
mL	millilitre
mMol or mM	Millimole
min	Minute
>	More than
M	Molarity
nm	Nanometer
cm ⁻¹	Per centimeter
ppm	Part per million

$\% S_d$	Percentage of shrinkage in diameter
$\% S_t$	Percentage of shrinkage in thickness
$\% X_c$	Percentage of crystallinity
$\% Y_{Pt}$	Percentage of yield
θ	Theta
H_v	Vickers hardness
Wt. %	Weight percent

SINTESIS DAN PENCIRIAN PELBAGAI MULTIDOP (Mg^{2+} , Si^{4+} , Cu^{2+} , Fe^{3+}) HIDROKSIAPATIT KARBONAT MELALUI KAEDAH NANOEMULSION

ABSTRAK

Komposisi Hidroksiapatit disintesis (HA) hampir sama dengan mineral tulang semulajadi telah digunakan secara meluas untuk aplikasi bioperubatan seperti pengganti tulang, penyampaian ubat dan salutan untuk implan. Matlamat kajian ini adalah untuk mensintesis dan mencirikan pelbagai dop ion (Mg^{2+} , Si^{4+} , Cu^{2+} , Fe^{3+}) hidroksiapatit karbonat melalui pengemulsian nano untuk meningkatkan sifat-sifat fizikal, mekanikal dan biologi. Komposisi mula dikategorikan ke dalam [nCO_3^{2-}/nPO_4^{3-}] nisbah molar = 0.67 dan 1.00. Teknik-teknik pencirian bahan tipikal telah digunakan untuk menganalisis sifat-sifat fizikal dan mekanikal serta bioaktiviti hasil sintesis dan sampel tersinter. Keputusan yang diperolehi mengesahkan bahawa ion-ion dop telah dimasukkan ke dalam struktur kristal untuk membentuk karbonat HA jenis-B. Dengan [nCO_3^{2-}/nPO_4^{3-}] nisbah molar = 1.00 menunjukkan saiz zarah yang lebih kecil luas permukaan yang lebih luas besar kandungan CO_3^{2-} yang lebih tinggi daripada [nCO_3^{2-}/nPO_4^{3-}] molar nisbah = 0.67. Ujian mekanikal untuk sampel [nCO_3^{2-}/nPO_4^{3-}] molar nisbah = 1.00 pada pensinteran suhu 750, 800 dan 850 °C menunjukkan kekerasan dan nilai kekuatan tegangan dalam lingkungan tulang *cancellous*. Dalam ujian bioaktiviti *in vitro* telah menunjukkan apatit seumpama tulang terbentuk pada pelet tersinter berbanding serbuk as-sintesis. Sampel pelbagai dop tersinter mengandungi Mg^{2+} , Si^{4+} dan Cu^{2+} basan menunjukkan lebih pembentukan apatit selepas 21 hari berbanding dengan sampel kawalan. Kajian ion dan profil pH dari sampel tersinter menunjukkan keluaran yang stabil dan dos

selamat seperti yang terdapat dalam manusia. Hasil secara keseluruhan menunjukkan potensi kedua-dua serbuk nano dan sampel tersinter dalam aplikasi bioperubatan.

SYNTHESIS AND CHARACTERIZATION OF MULTI-DOPED (Mg²⁺, Si⁴⁺, Cu²⁺, Fe³⁺) CARBONATED HYDROXYAPATITE VIA NANOEMULSION

METHOD

ABSTRACT

Synthesized hydroxyapatite (HA) with composition close to the mineral phase of the natural bone has been widely used for biomedical applications such as bone substitute, drug delivery and coating for implants. The goal of this study was to synthesize and characterise of multi-dope (Mg²⁺, Si⁴⁺, Cu²⁺, Fe³⁺) carbonated hydroxyapatite via nanoemulsion route to enhance its physical, mechanical and biological properties. The compositions were categorized into $[n\text{CO}_3^{2-}/n\text{PO}_4^{3-}]$ molar ratio = 0.67 and 1.00 based on the carbonate content. Typical materials characterisation techniques were used to analyze the physical and mechanical properties as well as the bioactivity of the as-synthesize and sintered samples. The result confirmed that these doping ions were incorporated within the crystal structure to form B-type carbonated HA. The $[n\text{CO}_3^{2-}/n\text{PO}_4^{3-}]$ molar ratio = 1.00 revealed a smaller particle size, higher surface area and higher CO₃²⁻ content compared to $[n\text{CO}_3^{2-}/n\text{PO}_4^{3-}]$ molar ratio = 0.67. Mechanical test for $[n\text{CO}_3^{2-}/n\text{PO}_4^{3-}]$ molar ratio = 1.00 samples at sintering temperatures of 750, 800 and 850 °C showed hardness and tensile strength values in the range of the cancellous bone. *In vitro* bioactivity revealed a more bone like apatite in the sintered pellets compared to the as-synthesize powders. The sintered multi-doped samples containing Mg²⁺, Si⁴⁺ and Cu²⁺ showed more apatite formation after day 21 compared to the other samples. The ion release study and pH profile from the sintered samples showed a stable release within the range found in human. The result as a whole shows the potential of both the nanopowders and sintered samples in the biomedical applications.

CHAPTER ONE

INTRODUCTION

1.1 Research background

The most widely used augmentation surgical transplants in orthopedic is bone graft with close to quarter billion procedures being performed annually. Bone graft is ranked next to blood transfusion as the world's second most transplanted tissue that requires high clinical regeneration standards such as osteoconduction, osteoinduction, and osteogenesis (Wang and Yeung, 2017). Though autologous bone grafting, a term use to describe graft from patients' own body, have shown properties similar to the gold regeneration standard nevertheless donor site morbidity and availability have to be considered (Pape et al., 2010). Allografts (graft from another person) and xenografts (graft from animals) have demonstrated properties such as osteoconductivity and limited osteoinductivity in demineralized bone matrix form (Fillingham and Jacobs, 2016). However, high risk of disease transmission and infections, availability, and poor healing ability compared to autologous grafts have been the challenge (O'Brien, 2011). These inherent issues have brought to fore alternative synthetic bone graft and substitute (BGS) such as synthesized biomaterials and biological factors (Wang and Yeung, 2017). Thus, bone tissue engineering (BTE) techniques presents innovative ways of reducing the problems created by conventional grafts using tailored scaffold and bone graft designs with enhanced osteogenicity, osteoconductivity, and osteoinductivity (Oryan et al., 2014a).

The natural bone provides a sophisticated load bearing architecture for the entire human organs. In addition, it serves as a protection shield for internal organs, a repository of biominerals and provides the muscular framework for mechanical

mobility (Feng and Thian Eng, 2013). The dynamic and plastic nature of bone in human body is remarkable. Numerous parameters such as mass, age, physical movement, hormonal balance, calories level, and ecological elements can alter the shape and structure of bone (Mazzotti and Ruggeri, 2016). The strength of intracranial bone had been demonstrated to reduce strains and energy vibration to the brain during severe impact. The natural bone has tougher mechanical properties compared to other delicate organs such as the lungs (Kokubo and Takadama, 2006). Despite excellent biomechanical properties, the natural bone is prone to pathological diseases and trauma-induced fracture. On top of the list of bone fracture problems are hips, ankles, tibia and fibula with the U.S alone projected to have over 500,000 hip fracture cases per year in 2050 (Huang et al., 2017). The occurrence of osteoporosis diseased bone in the EU was 27.6 million in 2010 while the annual rate of bone fracture was projected to increase by about 28% from 3.5 million to 4.5 million in the year 2025 (Wagoner Johnson and Herschler, 2011). The relative prevalence of osteoporosis in Asian population compared to Western nations is attributed to lower body mass index (BMI) and height associated. In 2005, approximately 24.1% of Malaysia population was documented of having trauma and fragility related bone fracture cases, with more of hip fracture observed amongst Chinese and Malays compared to the Indian group (Abdulameer et al., 2017).

Globally, bone fracture cases attributed to road-traffic injury and the impact on societal and economic costs is on the rise. The Global Burden of Diseases, Injuries, and Risk Factors conducted in 187 nations from 1980 to 2010, revealed an increase in mortality rate of 9.6% from 8.8% within two decades. This was linked to a 46% increase of the world death caused by road traffic accident (Pan et al., 2014). Besides high-energy trauma like road accidents and explosions or pathological cases of

orthopedic fracture, low energy factor such as fall account for significant amount of bone fracture. Study in Malaysia showed that low energy bone fracture leading to morbidity and disability occur mostly at home between the hours of 10am to 11pm. It further highlighted that the commonest method of fracture for children trauma was fall (77.2%) trailed by road accident (10.8%), sports (7.0%) and others (0.8%) (Bhardwaj et al., 2017). This increase of combine cases of high or low energy trauma and pathological orthopedic fracture has seen an increase in the use of bone grafts.

[paragraph] The most commonly used BGS are calcium phosphate CaP biomaterials (hydroxyapatite; HA, tricalcium phosphate; TCP, CaP cements) and recombinant human bone morphological proteins (rhBMPs) biological source (Kurien et al., 2013). The use of engineered biomaterials has been shown to eliminate the risk of immunogenicity, minimize cycles of surgery, and can readily be produced *en masse* (Kohli et al., 2018).

Biomaterials serve as a vital factor of tissue engineering designed to provide the necessary interface for local extracellular matrix cell growth and eventual tissue regeneration. Tailoring biomaterials mechanism in a manner similar to the intended native surroundings relies upon the understanding of the natural bone. The point of interest has been on addressing biomimetic surface topography for influencing cell behavior, managed transport of bioactive signals to stimulate regeneration, bone assemble vascularization, articular cartilage zonal structure, and osteochondral interface integration (Lee et al., 2014).

Engineered biomaterials are ones that have been designed for specific purposes or have qualities that make them suitable for a given application. There are a great number of these materials utilized in biomedical applications, for example, ceramics (calcium orthophosphate ceramics, CaP; bioglass systems; glass-ceramics),

polymeric materials (polyethylene, PE; poly-ether-etherketone, PEEK; polylactic-co-glycolic acid, PLGA), and metals (titanium, stainless steel, and its alloys, and cobalt chromium alloys) (Reit et al., 2017). Metals alloys possessed high corrosion resistance, while concerns with the biocompatibility of cobalt chromium wear debris in orthopedic applications and crevice corrosion remains a challenge. Polymer and ceramics biomaterials have no issues with biocompatibility of wear debris as well as corrosion. While the wide range in biomechanical properties of polymers have increased its applications in orthopedic applications, it presents the risk of degradation and leaching due to polymerization process.

On the other hand, in spite of the relatively high brittle index, ceramics are the most preferred alternative to metals in orthopedic applications because of its excellent qualities: such as high resistance to *in vivo* corrosion, biocompatibility risk free and high modulus (Reit et al., 2017). Bioceramics further offer other pertinent sets of properties that distinguished it from other biomaterial candidates such as water contact angle of 60–85° which prevents conformational changes in adsorbed plasma proteins and thus easily support cell-ligand binding; relatively inexpensive fabrication and storability; and versatility of shape and sizes (Kong et al., 2015).

The use of a synthetic bone substitute in biomedical has vastly increased yet the regeneration qualities compared to autologous bone grafts is still inferior due to the absence of osteoinductive property (Wang and Yeung, 2017). The orthopedic application challenge for one the most used bioceramics, CaP (and other ceramics) is poor seeding of osteogenic cells such as mesenchymal stem cells onto the appropriate scaffolds and subsequent implantation of the seeded scaffolds into the bone defect (Daculsi, 2014). Therefore, to improve the conventional bioceramics properties in bone graft applications, ion doped in CaP ceramics like HA amongst

others has been researched and reported to demonstrate enhanced biological responses such as osteogenesis and angiogenesis (Birgani et al., 2017).

The substitution of ionic species such as CO_3^{2-} , F^- , Mg^{2+} , Sr^{2+} , $\text{Fe}^{2+/3+}$, Si^{4+} , Cu^{2+} , Li^+ , Zn^{2+} , Mn^{2+} and Co^{2+} , into bone graft materials offers a cheaper and viable result for bone defect regeneration (Wang and Yeung, 2017, Xia, 2013). These bioinorganic ions such as Mg^{2+} creates an unstable bioactive HA crystal structure thus enabling rapid cell induced bioresorption, remodeling/new bone formation, water interaction and osteogenic ability (Kurien et al., 2013). *In vivo* studies showed an excellent biocompatibility, angiogenesis and vascularization for copper ion; reduction in tumor volume with low toxicity for iron ion; superior bone/implant attachment, neovascularization and cell infiltration for silicon ions (Kattimani et al., 2016).

1.2 Problem Statement

Given a similar chemistry to the inorganic phase of biological hard tissue, synthetic HA has been successfully applied as artificial bone constructs in certain cases. However, HA typically fails to serve as efficiently as natural bone due to lack of essential physiological natural bone impurities such as the 4–8 wt.% of CO_3^{2-} (responsible for B-type CHA) and trace elements. Thus, improved B-type carbonated HA *in vivo* solubility and bio sorption leading to early bone growth compared to HA has been established (Bang et al., 2014a). Models involving varying compositions have shown that engineering of synthetic bone graft bioceramics with ions found in the natural bone would enhance its physico-chemical properties (Combes et al., 2016). Hence, latest research developments focus on the incorporation of bioinorganic ions that increase the overall performance of CaPs to

have the potential to stimulate new bone formation (osteinductivity) (Bose et al., 2013b).

However, the ability to stimulate osteogenesis or bone regeneration must additionally be coupled with angiogenesis or blood vessel formation as these approaches are intricately related and osteogenesis would not be feasible without angiogenesis (Bose et al., 2013b). Although single or dual dopants have been incorporated into HA to elicit bone growth responses (Landi et al., 2010, Furko et al., 2018), there is yet any research on tailored ternary or quaternary ion doping on B-type carbonated HA tailored to induce combined osteogenic and angiogenic properties. Thus, this research focus on the development of multi-ionic (Mg^{2+} , Si^{4+} , Cu^{2+} , Fe^{3+}) doped B-type carbonated HA at nanopowder for coating/bone fillers applications and solid state for load bearing at sintering temperatures of 750, 800 and 850°C respectively.

1.3 Scope of study

The scope of this study covers the synthesis and characterization of multi-doped B-type carbonated HA bioceramics from high-purity chemical precursors by nanoemulsion route. Furthermore, the mechanical properties and *in vitro* bioactivity were explored as outlined in the flow chart below (Fig.1.1).

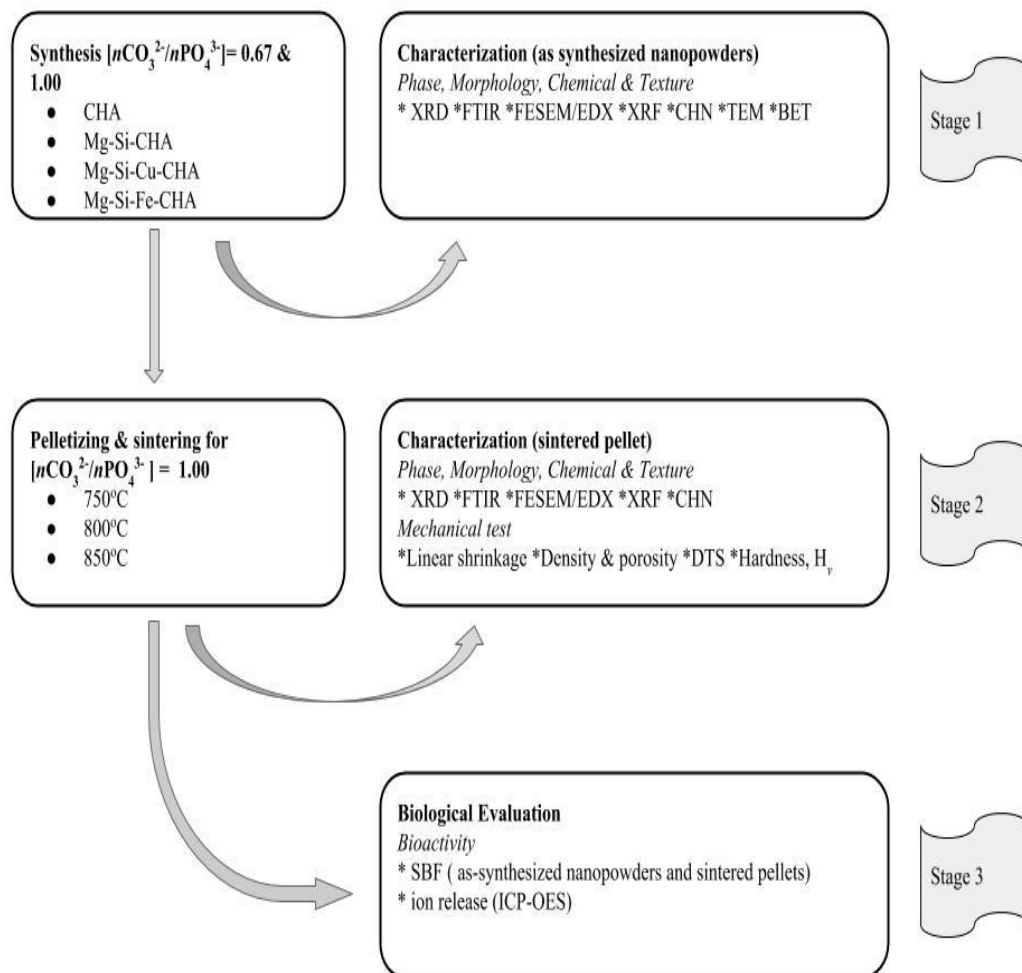


Figure 1.1 Flow chart of the research containing three stages of execution.

1.4 Research Objectives

1. Developing and characterizing (physical and mechanical properties of multi-dope B-type carbonated hydroxyapatite with multi-ionic species such as Mg^{2+} , Fe^{3+} , Cu^{2+} and Si^{4+} using the nanoemulsion route (wet method).
2. Evaluating the in vitro bioactivity and ion release of the as-synthesized nanopowders and sintered pellets in simulated body fluid.

1.5 Thesis outline

The introduction in Chapter 1 explains the research background and presents the problem statement, research objectives, scope of the study and the thesis structure. In Chapter 2, current background literature is explained with emphasis made on bone minerals, multi-ionic substituted HA, methods of synthesizing carbonated HA thermal treatment studies. The materials and methodology with a robust discussion on preparation and characterization presented in Chapter 3. Chapter 4 offers a comprehensive discussion from the results obtained. In the end, conclusions and recommendations for future studies are highlighted in Chapter 5.

CHAPTER TWO

LITERATURE REVIEW

2.1 Introduction

A bone usually gets fractured completely or partly in many instances from trauma due to fall, vehicle accident or sports while pathologies such as osteoporosis may create thinning of the bone in older people making the bone susceptible to fracture (Valley, 2017). The capacity to make bone-like materials with regenerative functions for the treatment of damaged or diseased bone throughout human history was nonexistent until the inventions of third generation biomaterials (Fig. 2.1).

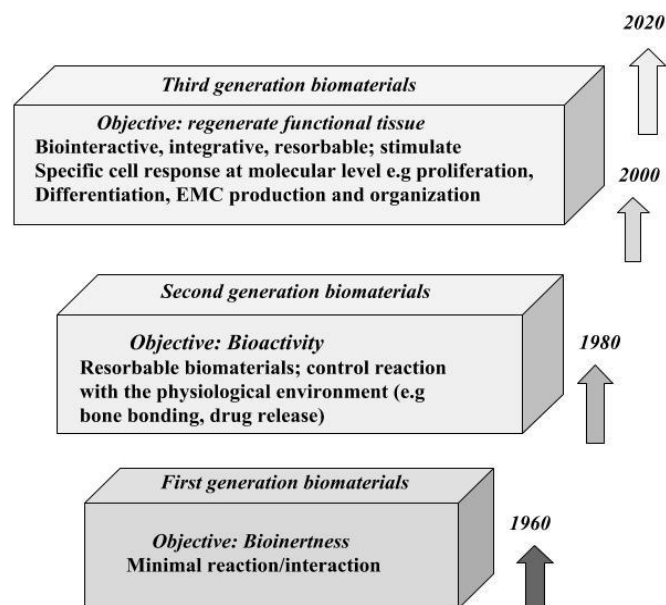


Figure 2.1 Generation of biomaterials and timelines (Lemons, 2013).

This new third generation biomaterial became the clinically improved versions of the earlier first and second-generation biomaterials developed in the 1950s and 1980s

with mere biocompatibility and bioactive properties respectively (Ratner et al., 2013). The advent of third-generation biomaterials over the past decade such as metals, polymers, bioglasses, calcium carbonates and calcium phosphates (CaPs) are finding increasing applications in bone repairs and regeneration (Xu et al., 2017a).

This chapter attempts to review biomaterials with emphasis on bioceramics as a biomedical material as well as related discussion on human bone composition, minerals and structure.

2.1.1 Bone

Bone constitute of a rigid body tissue of cells embedded in an abundant hard intercellular material. The two principal components of this material i.e. collagen and calcium phosphate, distinguish bone from such other hard tissues as chitin, enamel and shell. Bone tissues make up the individual bones of the human skeletal system and the skeletons of other vertebrates (Whedon and Heaney, 2018). The bone is amongst few organs that can regenerate and repair itself: in several cases, bone injuries and fractures restoration occur completely scar-free. In pathological fractures or immense bone defects, however, bone fails to heal itself. Combine effect of poor blood flow, bone and surrounding bone tissue infection can inhibit the healing of the bone thus creating slow or non-union of the fracture tissue (Oryan et al., 2014b).

Structurally, the bone comprises of marrow cased in a periosteum. The macrostructural bone consists of 80% the cortical (mainly dense) and 10% trabecular or cancellous (mainly porous) while the microstructural skeletal comprises of randomly arranged collagen fibers which calcified into woven lamellar bone (Lee et al., 2014). The strength of human bone result from a combination of several elements such as bone mineralization degree, HA crystal size and heterogeneity, collagen

features, osteocyte density, cancellous and cortical microstructure, and hard tissue geometry. These elements of bone strength may autonomously contribute to the increased or decreased risk factors associated with bone fracture (Fonseca et al., 2014). The functions of the bone are achieved by three important cells namely osteoblasts, osteoclasts, and osteocytes. Osteoblasts are task with osteogenic functions originating from mesenchymal, while osteoclasts are responsible for bone resorptions and osteocytes (transitioned matured osteoblast) are charge with mechanosensors and mineral homeostasis functions (Del Fattore et al., 2012).

2.1.2 Composition of Bone

The natural bone composition can be defined in terms of the mineral phase HA ($\text{Ca}_{10}(\text{PO}_4)_6(\text{OH})_2$), an organic phase and water (Fig. 2.2). The mineral phase is typically about 70%, while the organic phase constitutes the remaining 30%. The amount of each component is largely affected by factors such as age, size, gender, disease and treatment (Boskey, 2013, Alvarez and Nakajima, 2009).

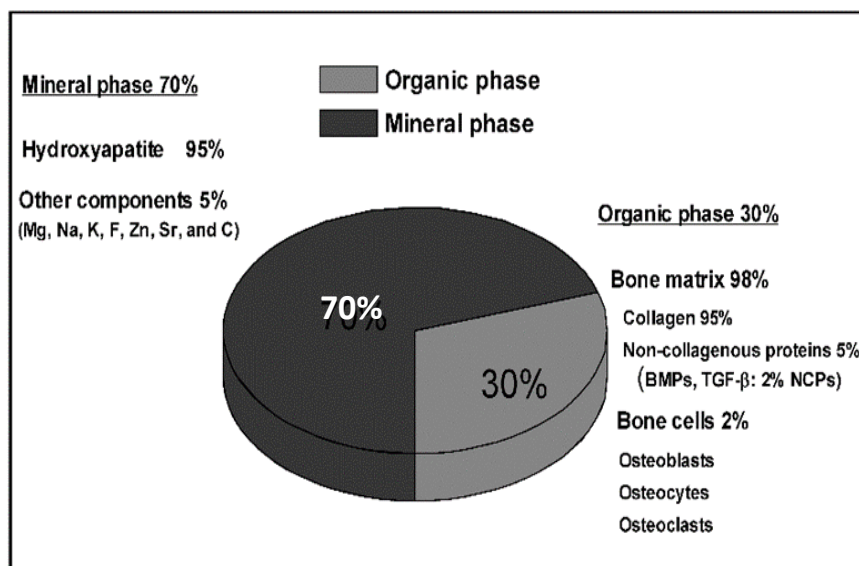


Figure 2.2 Displayed matrix of organic and inorganic component of bone composition (Alvarez and Nakajima, 2009).

2.1.3 Macrostructure of bone

At the macro scale, human bone has been classified into five major types (Fig. 2.3), namely long bones (femur, tibia, ulna and radius), short bones (carpal bones of the hand), flat bones (skull, sternum and scapula), irregular shaped bones (vertebra and ethmoid), and sesamoid bones (bones embedded in tendons). These bone are the mainframe that performs the load bearing and protective functions of other soft tissues in the human body (Umadevi and Geethalakshmi, 2011).

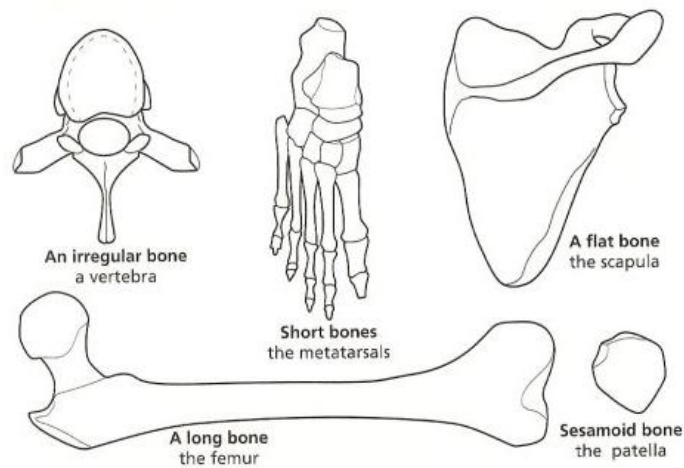


Figure 2.3 The types of human bone according to shape

The embryonic development stage of bone creates mechanisms such as endochondral and intramembranous responsible for the development of long and flat bones respectively. The combined matrix of long and flat bones is embedded with a dense thin outer section known as the cortex or cortical bone. As illustrated in Fig. 2.4, within the cortical bone is a cavity of marrow with features such as hematopoietic elements, fat and spicules of bone. The cancellous (spongy or trabecular) is what is simply termed spicule bone (Khurana and Safadi, 2010, Rho et al., 1998).

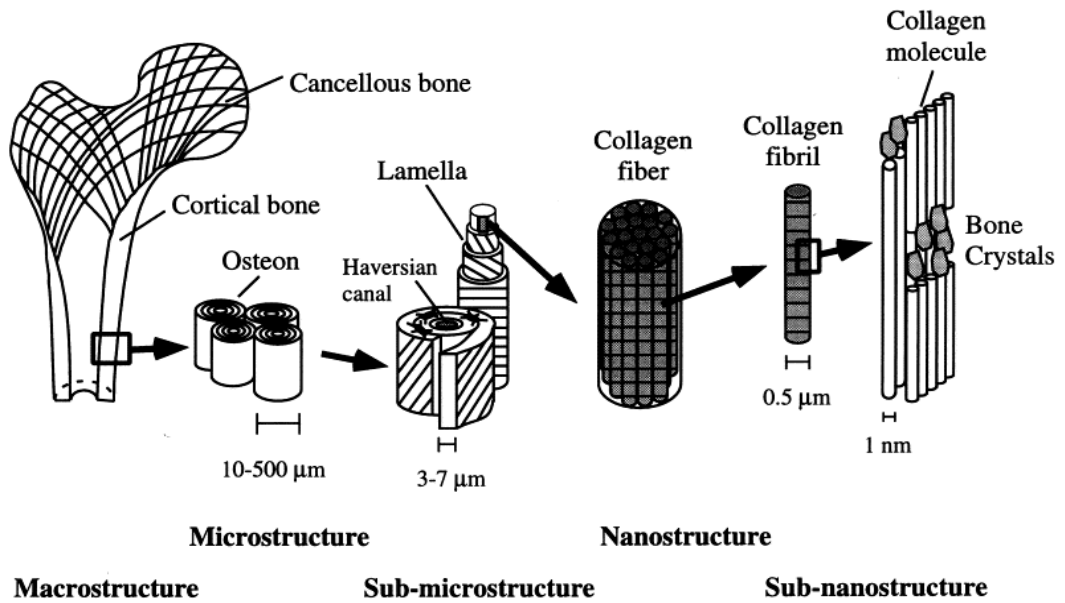


Figure 2.4 The macro to sub-nanostructure ordered arrangement of the human bone (Rho et al., 1998).

2.1.4 Microstructure of bone

The microstructure of the human bone as shown in Fig. 2.4 comprised of planar patterned of 3 to 7μm broad lamellae formed from mineralized collagen fibres. The osteon or Harversian system is thus formed from these clusters of lamellae coaxially wrap around a central canal of the cortical bone. Osteons formed from cortical bone are distinguished from non-harversian cortical bone (woven bone), by their typical cylindrically lining parallel to the long axis of the bone (Rho et al., 1998). In contrast, the microstructure of trabecular bone is organized like fibre texture of mineral platelets arranged parallel to the same path as collagen's fibres (Eliaz and Metoki, 2017). The microstructure level of bones is an important

determinant of biomechanical properties and particularly defines the way hard tissue is spatially organized.

Bone resorption properties of bone rely on the size of the surface-to-volume ratio (SVR) of trabecular bone: larger SVR leads to increased resorption and vice versa. Increase in SVR also decreases the cancellous bone volume (CBV) by gradually thinning thereby shifting from a plate-like shape to a rod-like shape, losing spongy connectivity and eventually causing bone deterioration. Research on volunteers aged between 20 to 90 years indicates a mean decrease of about 27 % in cancellous bone volume (CBV) in the distal radius of female and male (Khurana and Safadi, 2010). The characterization of the microstructure of bone by histomorphometry has been enhanced by microcomputed tomography (micro CT) capable of assessing the three-dimensional (3D) trabecular bone microarchitecture (Fonseca, 2012).

2.1.5 Nanostructure of bone

The nanoarchitecture of bones comprised of lamellae with mineralized collagen fibril in the nanometric region of about 100 nm in diameter and be can be termed the core unit of the bone material. The length and thickness of fibrils molecules are approximately 300 and 1.5 nm which are primarily best, describe as an organic base matrix. The formation of apatite depends on the distinct boundaries of the collagen molecules secreted by osteoblasts and their aftermath regrouping. The crystal growth emanating in the bone domain is largely controlled by collagen in the fibrils through series of discrete and discontinuous restriction. The isotropic attributes in bone that hinder crack propagation and enhance toughness are fundamentally controlled by the organization of nanodimension fibres of both lamellae and collagen (Eliaz and Metoki, 2017). The understanding of the

nanoarchitecture such as collagen fibrils and apatite crystals of bone has been possible by Transmission electron microscopy (TEM). The mineral phase is essentially inorganic material of carbonate-substituted HA nanocrystals with plate-like shape, with an average thickness of about 2– 7 nm, length ;15–200 nm, and width;10–80 nm (Fonseca, 2012).

2.1.6 Bone Cell

Osteoblasts, osteocytes and osteoclasts (Fig. 2.5) can be regarded the most important bone cells and are explained in the section below.

2.1.6 (a) Osteoblasts, Osteoclasts and Osteocytes

Osteoblast refers to cells that mineralizes bone in the cause of early formation and subsequent bone remodeling process. The formation of this cells involves staking of packed sheet on the surface of the bone where cellular activities spread through the evolving bone. These cells are product of differential osteogenic cells in the periosteum, the tissue that clads the outer surface of the bone, and in the endosteum of the marrow cavity. (Rogers, 2010). *Osteoclasts* refers to a multinucleated cell that are involved with bone dissolution and absorption. To response to structural stress and calcium requirement, bone tissue systematically breaks down and remodeled through osteoclasts mediation. This process entails fragmentation and digestion of bone minerals by osteoclast with its cytoplasmic vacuoles. Bone minerals such as calcium and phosphorus are released into the blood and osteoid (unmineralized bone) is buffered from osteoclastic resorption (Rogers, 2010). Osteocytes are cells that spread within the constituent of a mature bone. *Osteocytes* arise from osteoblasts that transformed into enclosed organic matrix

entrenched in the bone. They occupy a pocket-like space called lacunae through which tiny canaliculi are transmitted with other osteocytes and osteoblasts interface. The canaliculi create a large surface area upon which Calcium and phosphorus ions can exchange between plasma and bone (Feher, 2017).

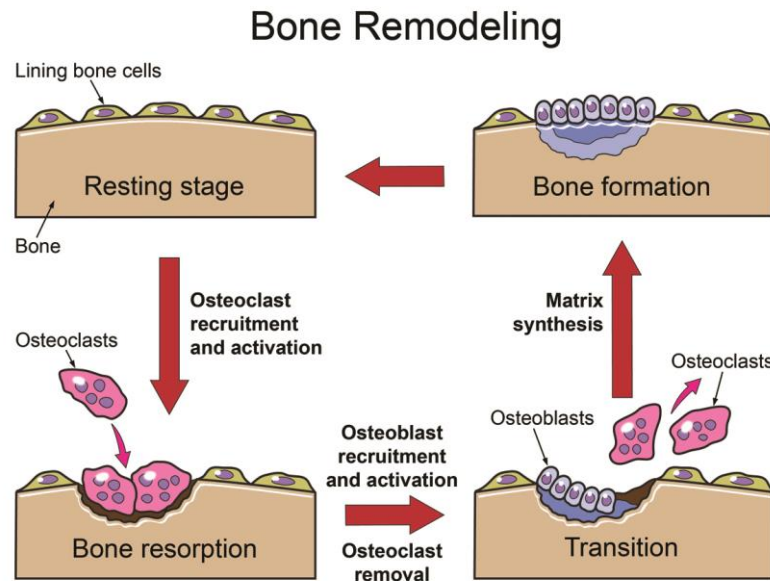


Figure 2.5 Bone cells remodeling process: osteocyte, osteoblast and osteoclast (Rogers, 2010).

2.1.7 Biomechanical Properties of Bone

This quality is best described from the bone tissue cortical and cancellous bone systems. A key characteristic of cortical bone mechanical properties is its stronger and stiffer but shorter fatigue life and lower toughness compared to remodeled secondary bone. Microstructure and mechanical properties like stress and strain distribution of the bone can be affected by apparent density. The apparent density of cancellous bone apparent density is largely affected by its microstructure

orientation and organization. Thus, mechanical anisotropy in the bone can orient with consistent loading direction (Fyhrie, 2010).

The measurement of cortical bone can be carried out with testing techniques such as: uniaxial compressive or tensile testing, or three or four-point bending. The mechanical features of cortical bone such as high degree of anisotropy and vary between gender, bone location, testing environment (dry or wet), age and health. The challenge of measuring properties of trabecular bone is far more is due to the small dimensions of the individual trabeculae (Alvarez and Nakajima, 2009). Thus, mechanically cortical bone material's properties differ from trabecular bone as shown in Table 2.1.

Table 2.1. Human cortical and trabecular bone: selected mechanical properties (Alvarez and Nakajima, 2009)

Cortical Bone	Shear Strength	Strength	Young's Modulus
	$\times 10^6 \text{ N/m}^2$	$\times 10^6 \text{ N/m}^2$	range $\times 10^9 \text{ N/m}^2$
Compression test	–	219 \pm 26 Longitudinal 153 \pm 20 Transverse	14.1 – 27.6
Tensile test	–	172 \pm 22 Longitudinal 52 \pm 8 Transverse	7.1 – 24.5
Torsional test	65 \pm 9	–	–
Ultrasonic method	–	–	22 – 24.5
Trabecular Bone	Shear Strength	Strength	Young's Modulus
	$\times 10^6 \text{ N/m}^2$	$\times 10^6 \text{ N/m}^2$	range $\times 10^9 \text{ N/m}^2$
Compression test	–	1.5 – 9.3	0.1 – 0.4
Tensile test	–	1.6 – 2.42	10.4 \pm 3.5
Torsional test	6.35 \pm 2	–	–
Ultrasonic method	–	–	14.8 \pm 1.4

2.2 Types of Bone Substitute

Traumatic injury ranks high as the main cause of global mortality and disability across all spectrum. A forecast by the World Health Organization (WHO) shows that the global number of people living to 85 and older will increase by 351% in the next four decades. The implication of this rise in the number of old people is a rise in the number of people suffering from severe health issues such as osteoporosis and bone fracture from low energy trauma (Roy et al., 2015). Osteoporotic fracture study revealed that cases leading to higher morbidity, mortality, and costs stems majorly from a hip fracture. It projected that approximately 4.50–6.26 million of the global hip fractures will occur by 2050 and Asia will have 50% of these cases. The direct cost of hip fracture in Asia will rise from US\$9.5 billion in 2018 to US\$15 billion in 2050. Malaysia and Japan are reported to have the highest and the lowest increase in the total number of hip fracture, respectively (Cheung et al., 2018). The data from the United Nations pointed out the median age in Malaysia and Japan at 26.99 years and 45.53 years in 2012. Therefore, the occurrence of hip fracture in Malaysia is predicted to be lower than that in Japan. China and India with combined 37% of the global population contribute to the highest absolute number increase in hip fracture due their highest population size (Cheung et al., 2018). Hence, hip fracture is expected to be an enormous burden for Asia needing urgent interventions.

Also, a separate study estimated that there were 4.48 million people globally who suffered from disability because of bone fractures in 1990. In Europe, about 1.75% of the entire burden of disease is attributed to osteoporotic bone fractures (Roy et al., 2015), and osteoporosis is costing the US is a startling US\$17–20 billion. Consequently, a major effort such as improve diagnosis and medications, numerous fracture prevention strategies, and research, has been undertaken to curb the

occurrence of fracture globally. Among such research employed in the treatment of damaged and diseased bone in recent time is a bone substitute.

2.2.1 Bone Graft Substitute (BSG)

Bone substitute can be referred to as “an artificial, inorganic or biologically organic matrix which can be inserted for the treatment of a bone defect instead of autogenous or allogeneous bone” (Schlickewei and Schlickewei, 2007). Diverse bone substitutes have found applications in biomedical engineering for the past several decades. They had been classified into (i) bone grafts (autograft, allograft, xenograft) and (ii) ceramics (HA, TCP, CaS). The important criteria to be considered for the ideal bone are; biocompatible with the non-inflammatory response, easily moldable into the with brief setting time, osteoconductive, osteoinductive, resorbable, thermally nonconductive, sterilizable, availability and cost-effective (Campana et al., 2014).

The synthetic bone graft substitutes are chemically prepared in the laboratory with tailored properties close to the human bone (Adham et al., 2015). Another classification of bone grafts based on bone tissue response *in vivo* are, (a) osteoconductive grafts (b) osteoinductive grafts and (c) osteogenic grafts. In osteoconductive, the grafting attaches readily to cells such as osteogenic and osteogenic thereby creating interconnected features, which favors cell migration and vessel formation. In an osteoinductive graft, the non-differentiated stem cells or osteoprogenitor cells is induced into differentiate state and ultimately into osteoblasts. Osteogenic cells refer to the cells of bone grafts that thrive during implant and form new bone at the recipient site (Nandi et al., 2010).

Table 2.2. Summary of biological properties of natural bone grafts and bone substitutes in the clinical application (Wang and Yeung, 2017)

Bone Graft Substitute (BSG)		Osteoconduction	Osteoinduction	Osteogenesis	Osteointegration	Structural support	Disadvantages	Clinical Applications
Autologous Bone Grafts	Autologous Cancellous	+++	+++	+++	+++	-	Limited availability and donor site morbidity	Bone defect, delayed union/non-union, discectomy, arthroplasty
	Autologous Cortical	+	+	+	+	+++	Same as above	Bone defects, discectomy
	Allogeneic Cancellous	+	+	-	++	-	Risk of disease transmission and immune reaction	Bone defects, delayed union/non-union, discectomy, arthroplasty
Allogeneic Bone Grafts	Allogeneic Cortical	+	-	-	+	+++	Sam as above	Bone defects, discectomy
	DBM	+	++	-	++	-	Variable osteoinductivity associated with donors and processing methods	one defects, discectomy, arthroplasty
Synthetic Bone Substitutes	Calcium sulfate	+	-	-	++	+	Rapid resorption, osteoconductive only	Bone void filler, bone graft extender
	Hap	+	-	-	-	++	Slow resorption, osteoconductive only	Same as above
	Calcium phosphate ceramic	+	-	-	+	++	Osteoconductive only	Same as above
	Calcium phosphate cement	+	-	-	+	+	Osteoconductive only	Same as above
	Bioactive glass	+	-	-	-	-	Bioactive osteoconductive only	Same as above
Polymethylmethacrylate PMMA		-	-	-	-	+++	Inert, exothermic, monomer-mediate toxic	Segmental bone defect, arthroplasty, vertebroplasty and kyphoplasty

Abbreviations: DBM, demineralized bone matrix; HA, hydroxyapatite; -, poor; +, good; ++, very good; +++, excellent

2.2.2 Autograft Bone Graft

Autografts, autologous, or autogenous bone grafts refers to grafts that are harvested and implanted from one site into another site within the same individual (Zimmermann and Moghaddam, 2011). This grafting can be trabecular or cortical (non-vascularized or vascularized) bone, and certain condition a mixture of both which contains active cells and osteoinductive proteins. Their absolute immunogenicity-free and retention of viability immediately after transplantation into host site distinguishes autograft to a ‘gold standard’ status. Moreover, they are optimally endowed with osteogenic, osteoinductive, and osteoconductive properties due to inherent presence of MSCs, osteoprogenitor cells, osteogenic cells, and growth factors (Oryan et al., 2014b).

In spite, the excellent qualities, drawbacks such as poor resorption, limited availability and viability are still linked to autografts. The merit of osteogenic, osteoconductive and osteoinductive properties is limited to a duration of 120 minutes from intra harvest to implant lest the cells perish. The tendency for ultrastructure alteration of the cancellous bone is high during autograft transplantation process, thus affecting ingrowth of vascularization and the permeation of early osteoblasts and osteoblast markers (Zimmermann and Moghaddam, 2011).

2.2.3 Allograft Bone Graft

Allograft bone is a viable alternative to autograft, it offers free donor site morbidity and finds high applications in revision arthroplasty surgery amongst others. Nevertheless, allograft comes with a challenge like transmittance infectious diseases (human immunodeficiency virus (HIV-1 and HIV-2), hepatitis B and C, syphilis and human T-cell lymphotropic virus (HTLV-1 and HTLV2)) and immunorejection reaction (Delloye et al., 2007). Stringent safety has been employed to

minimize disease transmittance and degradation such as serological testing, freeze-dried storing (-80°C), ethylene oxide, gamma-irradiation or thermal heat treatment. This safety although reduces the setback raised the also reduce mechanical and osteoinductive properties of the graft (Kurien et al., 2013). In addition, the allograft bone graft is confronted with procurement issues medically, legally and ethically in most part of the world (Poinern et al., 2014).

2.2.4 Xenogenic Bone Grafts

In xenogenics ‘de-protenized’ trabecular tissue is harvested from animals and transplanted to human recipients’ site. The lack of availability of human grafts prompted the use of xenografts are sterilized, processed or treated to serve as an effective compliment to other grafts. To avoid immunological response and pathogenic transmission the organic constituent of the xenogenic grafts must be entirely removed (Nazirkar et al., 2014). The useful inorganic content serves as organized matrix for new bone formation and a rich source of calcium, which is necessary for regeneration. In dentistry, xenograft based on processed bovine termed Bio-oss are presently in use. Also, composite of xenografts, growth factors and/or allografts are developed to mimic enhanced autologous graft (Nazirkar et al., 2014). Xenografts are abundant but are prone to the risk of rejection like allograft and faced with ethically and religious prohibition in the case of Islamic, Jewish and other belief systems (Iis and Faturrahman, 2009).

2.2.5 Synthetic Bone Graft

The severe scarcity of natural bone grafts and the unsustainability of such source for an increasingly ageing global population has prompted a vibrant market of bone grafts and substitutes (Wu et al., 2014). Since the early application of calcium

sulphate in the 1890s, bioceramics (alloplastic) have improved into newer synthetic bone graft substitutes such as calcium phosphate, tricalcium phosphate, composite bioceramics and bioactive glass. They are a viable alternative to natural bone grafts with an excellent fabricability range such as pellets, blocks, injectable putty and scaffold (Fillingham and Jacobs, 2016). Another synthetic variant is the polymer-based bone graft which can be degradable and nondegradable form alone or in combination with other materials, for instance, porous polylactic acid polymer (Kumar et al., 2013). Synthetic bone graft substitutes or alloplastic is gaining greater relevance where the source of the bone graft may be objectionable to patients' religious, ethical and/or cultural concerns. Patient's right is enshrined in most constitutions around the world to have an opinion on bone grafts due to philosophical or religious principles (Fernández et al., 2015).

2.3 Biomaterials

The European Society for Biomaterials (ESB) in 1976 viewed biomaterials as 'a nonviable material used in a medical device, intended to interact with biological systems'; this view later changed to a 'material intended to interface with biological systems to evaluate, treat, augment or replace any tissue, organ or function of the body'. Today these descriptions on biomaterials have evolved into materials which can elicit responses beyond interacting with the body to inducing biological processes into tissue regeneration (O'Brien, 2011).

The most acknowledged description of biomaterials is presently advanced by the American National Institute of Health (ANIH) that defines biomaterial as "any substance or combination of substances, other than drugs, synthetic or natural in origin, which can be used for any period of time, which augments or replaces partially or totally any tissue, organ or function of the body, in order to maintain or

improve the quality of life of the individual’’. The limitation of this definition is that it excludes materials such as orthodontic brackets and surgical devices (Bergmann and Stumpf, 2013).

Traditional biomaterials are categorized into four categories namely ceramics, polymers, metals and composite: they expected to possess certain ideal requirements (Fig. 2.6).

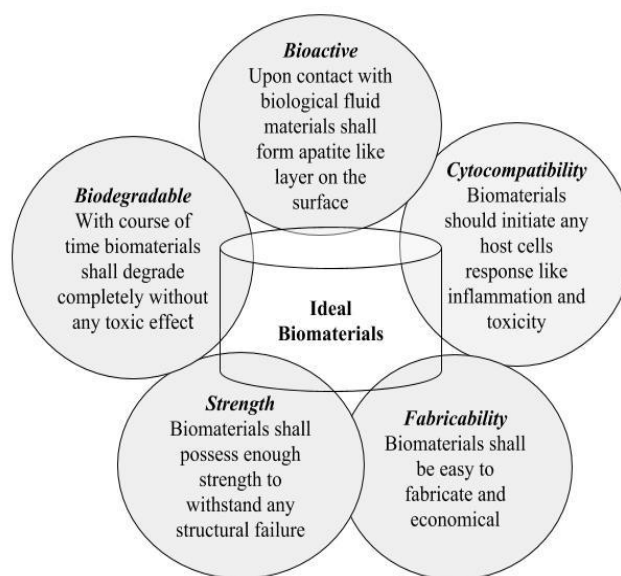


Figure 2.6 Requisite criteria for ideal biomaterials: bioactive, biodegradable, strength, fabricability and cytocompatibility (Kaur, 2017).

However, a current understanding of biomaterials has evolved more toward biomimetic/smart biomaterials, which mimic nature’s hierarchical structures. The research quest this day is in developing these categories of biomaterials with greater inherent qualities such as cytocompatibility, biodegradation, bioactivity, suitable mechanical strength, osteoinduction, and osteogenesis abilities (Kaur, 2017).